*URSI GASS 2021, Rome, Italy, 28 August - 4 September 2021*

# Recovery of Prior Information for Breast Microwave Imaging Using Neural Networks

Keeley Edwards*(1), Vahab Khoshdel(1), Mohammad Asefi(1), Joe LoVetri(1), Colin Gilmore(1), and Ian Jeffrey(1)
(1) Department of Electrical and Computer Engineering, University of Manitoba, Winnipeg, MB R3T 5V6, Canada

## Abstract

A recently developed neural network architecture for recovering the radius, height, and bulk complex-valued permittivity of the fibroglandular region of a human breast model from microwave measurements is extended to multiple frequencies. Results are presented for synthetic models with different sized fibroglandular regions both with and without a tumor present. The performance of this neural network architecture for single- and multi-frequency data in the 1.1 – 1.5 GHz range is demonstrated. Both neural networks are able to recover the desired bulk parameters of the fibroglandular region, with multi-frequency data leading to improved fibroglandular property estimates.

## 1 Introduction

Microwave imaging (MWI) shows promise for tumor detection and monitoring in breasts [1, 2]. At microwave frequencies, different breast tissue-types can generally be distinguished by their complex-valued permittivity [3]. When using inverse scattering-based approaches to the breast MWI problem, accurate prior information about the target is beneficial to successful reconstruction [4, 5, 6].

We have previously presented a synthetically trained neural network capable of recovering bulk parameters of grain stored in a large metal grain bin and have demonstrated its applicability for uncalibrated, experimental field data in two separate bin geometries [7]. Recently, we have applied this idea to breast imaging, using a single-frequency neural network to estimate the fibroglandular region of human breast models [8]. In this work, we extend that model to accept multi-frequency input data so as to compare the performance of the single- and multi-frequency networks.

## 2 Model Air-Based Breast Imaging Chamber

The human breast can be modelled as a fibroglandular region surrounded by an adipose region and covered with a layer of skin. The synthetic model used in this work uses a simplified breast model and the faceted air-filled breast imaging chamber presented in [9]. This chamber has 24 magnetic field probes designed to measure the $\phi$ component of the magnetic field along the chamber wall.

We assume that overall size and location of the breast can be fixed by a holder placed within this chamber. Following this assumption, the properties of the adipose region of the breast are assumed known, and the goal of the neural network is to recover only the bulk properties of the fibroglandular tissue. These bulk properties are parameterized into a four element vector, $\underline{\mathbf{p}}$, consisting of the real ($\varepsilon'$) and imaginary ($\varepsilon''$) parts of the complex-valued bulk permittivity, radius, and height of the fibroglandular tissue.

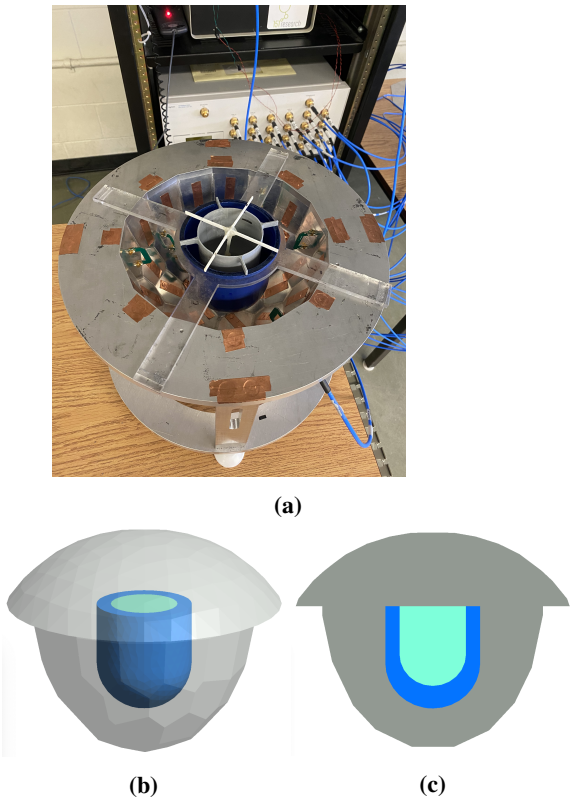

**Figure 1.** Experimental system (a) and synthetic model of the breast within the system with air (grey), adipose (dark blue) and fibroglandular (light blue) shown. The full chamber is shown in (b), and a cross section in (c).

## 3 Synthetic Data and Network Architecture

### 3.1 Labelled Data Generation

A discontinuous Galerkin method (DGM) forward solver is used to generate synthetic field data for the assumed model [10, 11]. Our previous work adopted a PEC lid

on the chamber [8], but here the top is modeled as an absorbing boundary condition to be consistent with future experiments. Each forward solver call generates a field data matrix, $H_\phi$, where each element, $H_{\phi i,j}$, is the measurement from the $i$th transmitter and $j$th receiver; the $i,i$ measurements are discarded and the matrix is flattened into a 552-element column vector. A multi-frequency, tumor-free, noise-free synthetic labelled dataset is generated by varying the size and permittivity of the fibroglandular region within a fixed adipose region.

## 3.2 Network Architecture

A fully connected neural network architecture that accepts $H_\phi$ data in either single- or multi-frequency format was developed. The single-frequency network accepts $H_\phi$ as a vector, whereas the multi-frequency network accepts the vertically concatenated $H_\phi$ vectors from each frequency of interest.

The architecture consists of 6 hidden layers, where the input size is $552 * n_f \times 1$, where $n_f$ is the number of frequencies used, as shown in Figure 2. All activations in the network are ReLU, and a residual sum of square errors loss function is used.

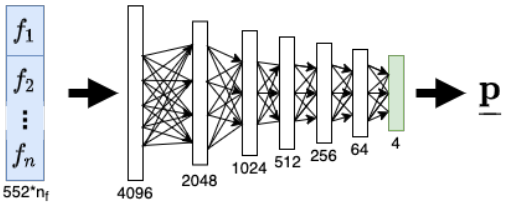


**Figure 2.** Network architecture. The size of each layer is shown under the vertical bar. The inputs are shown in blue, and the output layer is shown in green.

# 4 Results

## 4.1 Labelled Data Generation and Network Training

The tumor-free, noise-free, labelled synthetic data set consists of 7200 examples of different fibroglandular properties at each of five frequencies (1.1, 1.2, 1.3, 1.4, and 1.5 GHz). Table 1 describes the properties of the adipose and fibroglandular tissues represented in the dataset. The set is divided 85%, 10%, 5% into training, validation, and testing sets, respectively.

A single-frequency network using 1.1 GHz data, and a five-frequency network using 1.1–1.5 GHz data were trained. In both cases, the network was trained for a maximum of 150 epochs. An early stopping patience of 30 and a batch size of 100 were used.

**Table 1.** Summary of tissue properties represented in the labelled dataset.

| Tissue Type | | Radius [cm] | Height [cm] | $\varepsilon'$ | $\varepsilon''$ |
|---|---|---|---|---|---|
| Adipose | const. | 4.80 | 10.90 | 3.0 | - 0.6 |
| Fibro | min. | 2.85 | 5.30 | 15 | -25 |
| Fibro | max. | 4.10 | 9.80 | 25 | -15 |

## 4.2 Tumor Containing Test Set

While the goal of the network is to recover prior information about the breast tissue in the form of bulk parameters $\underline{\mathbf{p}}$ of the fibroglandular region, it is important that the network be robust to the presence of tumors within the breast. To evaluate the robustness of the network predictions, $\underline{\mathbf{p}}$, to the presence of tumors, a test set was created for three different sized fibroglandular regions; small, medium, and large. For each of these additional geometries, three test examples were generated: one without a tumor, and two with a 9 mm tumor in different locations $T1$ and $T2$. A fourth example was generated for the medium fibroglandular geometry, by placing a 4.5 mm tumor at position $T1$. Noise at -80dB was added to this data prior to using it to evaluate the trained networks. Results are presented in Table 2 (single-frequency) and Table 3 (multi-frequency).

**Table 2.** Fibroglandular parameter predictions from the single-frequency neural network.

| Position | Tumor [mm] | Radius [cm] | Height [cm] | $\varepsilon'$ | $\varepsilon''$ |
|---|---|---|---|---|---|
| Small fibroglandular case: | | | | | |
| True values: $\underline{\mathbf{p}}_{true}$ | | 2.90 | 5.35 | 20.00 | -21.60 |
| No tumor | - | 2.93 | 5.32 | 19.76 | -21.46 |
| T1 | 9 | 3.10 | 5.32 | 12.00 | -23.84 |
| T2 | 9 | 2.96 | 5.30 | 19.07 | -21.53 |
| Medium fibroglandular case: | | | | | |
| True values: $\underline{\mathbf{p}}_{true}$ | | 3.40 | 8.50 | 20.00 | -21.60 |
| No tumor | - | 3.40 | 8.43 | 19.50 | -21.75 |
| T1 | 9 | 3.41 | 8.46 | 19.20 | -21.76 |
| T1 | 4.5 | 3.40 | 8.48 | 19.72 | -21.65 |
| T2 | 9 | 3.41 | 8.46 | 19.56 | -21.89 |
| Large fibroglandular case: | | | | | |
| True values: $\underline{\mathbf{p}}_{true}$ | | 4.05 | 9.75 | 20.00 | -21.60 |
| No tumor | - | 4.03 | 9.76 | 20.09 | -21.91 |
| T1 | 9 | 4.03 | 9.77 | 20.11 | -21.91 |
| T2 | 9 | 4.03 | 9.77 | 19.88 | -22.00 |

As expected, the results show that the addition of higher frequencies in the multi-frequency network improves the network predictions for the smaller geometric features in the small and medium fibroglandular cases. In both the single- and multi-frequency case, the estimated parameters appear sufficiently accurate to suggest their use as prior informa-

**Table 3.** Fibroglandular parameter predictions from the multi-frequency neural network.

| Position | Tumor [mm] | Radius [cm] | Height [cm] | $\varepsilon'$ | $\varepsilon''$ |
|---|---|---|---|---|---|
| Small fibroglandular case: | | | | | |
| True values: $\underline{\mathbf{p}}_{true}$ | | 2.90 | 5.35 | 20.0 | -21.6 |
| No tumor | - | 2.90 | 5.30 | 20.34 | -21.50 |
| T1 | 9 | 2.91 | 5.30 | 19.97 | -22.04 |
| T2 | 9 | 2.90 | 5.30 | 20.21 | -21.64 |
| Medium fibroglandular case: | | | | | |
| True values: $\underline{\mathbf{p}}_{true}$ | | 3.40 | 8.50 | 20.0 | -21.6 |
| No tumor | - | 3.41 | 8.50 | 20.04 | -21.62 |
| T1 | 9 | 3.41 | 8.50 | 19.82 | -21.59 |
| T1 | 4.5 | 3.41 | 8.50 | 19.90 | -21.60 |
| T2 | 9 | 3.41 | 8.50 | 19.96 | -21.90 |
| Large fibroglandular case: | | | | | |
| True values: $\underline{\mathbf{p}}_{true}$ | | 4.05 | 9.75 | 20.0 | -21.6 |
| No tumor | - | 4.06 | 9.70 | 19.70 | -21.77 |
| T1 | 9 | 4.06 | 9.70 | 19.70 | -21.77 |
| T2 | 9 | 4.06 | 9.70 | 19.70 | -21.85 |

tion for subsequent tumor localization [6, 8].

## 5 Conclusion

We have presented a neural network for recovering bulk parameters of the fibroglandular region from synthetic microwave imaging data based on a model of the human breast. The proposed neural network architecture can be used for single- or multi-frequency data, and we have demonstrated that for certain fibroglandular geometries the use of multi-frequency data improves the neural network predictions. The networks are trained on synthetic data and appear to be robust to the presence of tumors. Current work is focused on applying these networks to multi-frequency experimental data and using the extracted bulk parameters as prior information for experimental tumor monitoring.

## 6 Acknowledgements

We would like to thank Nicholas Geddert for his support with the forward solver.

## References

[1] N. K. Nikolova, "Microwave imaging for breast cancer," *IEEE microwave magazine*, vol. 12, no. 7, pp. 78–94, 2011.

[2] L. M. Neira, B. D. Van Veen, and S. C. Hagness, "High-resolution microwave breast imaging using a 3-d inverse scattering algorithm with a variable-strength spatial prior constraint," *IEEE Transactions on Antennas and Propagation*, vol. 65, no. 11, pp. 6002–6014, 2017.

[3] M. Lazebnik, D. Popovic, L. McCartney, C. B. Watkins, M. J. Lindstrom, J. Harter, S. Sewall, T. Ogilvie, A. Magliocco, T. M. Breslin *et al.*, "A large-scale study of the ultrawideband microwave dielectric properties of normal, benign and malignant breast tissues obtained from cancer surgeries," *Physics in medicine & biology*, vol. 52, no. 20, p. 6093, 2007.

[4] N. Abdollahi, D. Kurrant, P. Mojabi, M. Omer, E. Fear, and J. LoVetri, "Incorporation of ultrasonic prior information for improving quantitative microwave imaging of breast," *IEEE Journal on Multiscale and Multiphysics Computational Techniques*, vol. 4, pp. 98–110, 2019.

[5] M. Asefi, A. Baran, and J. LoVetri, "An experimental phantom study for air-based quasi-resonant microwave breast imaging," *IEEE Transactions on Microwave Theory and Techniques*, vol. 67, no. 9, pp. 3946–3954, 2019.

[6] V. Khoshdel, M. Asefi, A. Ashraf, and J. LoVetri, "Full 3d microwave breast imaging using a deep-learning technique," *Journal of Imaging*, vol. 6, no. 8, p. 80, Aug 2020. [Online]. Available: http://dx.doi.org/10.3390/jimaging6080080

[7] K. Edwards, K. Krakalovich, R. Kruk, V. Khoshdel, J. LoVetri, C. Gilmore, and I. Jeffrey, "The implementation of neural networks for phaseless parametric inversion," in *2020 XXXIIIrd General Assembly and Scientific Symposium of the International Union of Radio Science*. IEEE, 2020, pp. 1–3.

[8] K. Edwards, V. Khoshdel, M. Asefi, J. LoVetri, C. Gilmore, and I. Jeffrey, "A machine learning workflow for tumor detection in breasts using 3d microwave imaging," *Electronics (Submitted to)*, 2021.

[9] K. Nemez, M. Asefi, A. Baran, and J. LoVetri, "A faceted magnetic field probe resonant chamber for 3d breast mwi: A synthetic study," in *2016 17th International Symposium on Antenna Technology and Applied Electromagnetics (ANTEM)*. IEEE, 2016, pp. 1–3.

[10] K. G. Brown, N. Geddert, M. Asefi, J. LoVetri, and I. Jeffrey, "Hybridizable discontinuous galerkin method contrast source inversion of 2-d and 3-d dielectric and magnetic targets," *IEEE Transactions on Microwave Theory and Techniques*, vol. 67, no. 5, pp. 1766–1777, 2019.

[11] N. Geddert, "An electromagnetic hybridizable discontinuous galerkin method forward solver with high-order geometry for inverse problems," 2020.